

Field theory description of ion association in re-entrant phase separation of polyampholytes

Jonas Wessén,¹ Tanmoy Pal,¹ and Hue Sun Chan¹

Department of Biochemistry, University of Toronto, 1 King's College Circle, Toronto, Ontario M5S 1A8, Canada

(*Electronic mail: jonas.wessen@utoronto.ca)

(*Electronic mail: tanmoy.pal@utoronto.ca)

(Dated: 25 April 2022)

Phase separation of several different overall neutral polyampholyte species (with zero net charge) is studied in solution with two oppositely charged ion species that can form ion-pairs through an association reaction. A field theory description of the system, that treats polyampholyte charge sequence dependent electrostatic interactions as well as excluded volume effects, is hereby given. Interestingly, analysis of the model using random phase approximation and field theoretic simulation consistently show evidence of a re-entrant polyampholyte phase separation at high ion concentrations when there is an overall decrease of volume upon ion-association. As an illustration of the ramifications of our theoretical framework, several polyampholyte concentration vs ion concentration phase diagrams under constant temperature conditions are presented to elucidate the dependence of phase separation behavior on polyampholyte sequence charge pattern as well as ion-pair dissociation constant, volumetric effects on ion association, solvent quality, and temperature.

I. INTRODUCTION

Numerous studies in the past decade have indicated that liquid-liquid phase separation (LLPS) of intrinsically disordered proteins (IDPs) or intrinsically disordered regions (IDRs) of proteins, often in the presence of nucleic acids and folded protein domains, is a critical physical mechanism behind the formation of biologically functional membraneless organelles such as the nucleolus, cajal bodies and stress granules^{1–13}. Electrostatics, among other multivalent interactions, is one of the major drivers of the biological LLPS because IDP/IDRs generally contain charged amino acid residues in their composition and are often polyampholytic in nature^{14–17}. In addition to a polyampholyte sequence's charge pattern—or more generally its charge composition—and concentration^{18–21}, the phase separation propensity of a specific polyampholyte depends on the condition of the solution determined by such factors as temperature^{22,23}, pressure^{22,24,25}, pH²⁶, as well as the concentration and type of salts present^{25,27}. Because of the charged nature of the polyampholytes, electrostatic interactions from the ion pairs in the solution affects its LLPS^{20,25,27,28} and could be a controlling factor in its bio-engineering²⁹. In general, an oppositely charged pair of ions can stay as solvated ions or they can form a chemically distinct complex, e.g. solvent-shared ion-pair, contact ion-pair, through association reactions depending on the solution condition. Although the effects of ion-strength on polyampholyte LLPS have been addressed by several analytical and computational studies, the consequences of ion-association has largely been unexplored.

In general, chemical reactions in biomolecular condensates are of broad interest because the regulation of biochemical reactions is one of several major biolog-

ically relevant functions of biomolecular condensates³⁰. Indeed, several recent computational studies have addressed phase separation in chemically reactive environments. For instance, the pH dependence of LLPS was studied by Adame-Arana *et al.* in a set-up where the net charge on the phase separating macromolecules is chemically coupled to the self-ionization of water²⁶. An investigation by Lin *et al.* elucidated the role of complex formation between the SynGAP and PSD-95 molecules in the LLPS of their mixture³¹. The study by Bartolucci *et al.* considered both equilibrium and fuel-driven phase separation of a polymeric component undergoing an internal molecular transition³². These studies provided valuable insights. However, they treated relevant interactions only up to mean-field theory (MFT) and did not incorporate amino acid sequence of the polyampholytes explicitly. Sequence specificity, and generally phase-separation driven by electrostatic interactions, are inaccessible to the aforementioned MFT approaches because of the non-negligible contributions from fluctuations^{20,33}; but these effects are physically and biochemically important. One of the goals of our present work is to develop theoretical approaches that allow these effects to be tackled.

Pinpointing the exact roles played by all the physical interactions affecting *in vivo* LLPS, or even its simplified *in vitro* counterpart, could be immensely difficult. For analytical and computational tractability, we consider a simple model where a polyampholyte species is phase-separating in the presence of two oppositely charged chemically reacting ion species A^+ and B^- . We assume that the concentrations of A^+ and B^- are in thermal equilibrium with the concentration of their charge-neutral product AB, following the balance equation



The dissociation/association constants K_d/K_a in Eq. (1)

are defined by

$$K_d = \frac{1}{K_a} = \frac{[A^+][B^-]}{[AB]}, \quad (2)$$

where $[X]$ is the equilibrium concentration of the species X ($= A^+, B^-, AB$). The reaction (1) could be used to describe several chemical processes including self-ionization of water, dissociation of weak organic acids (e.g. formic acid, acetic acid or carbonic acid) in the solution, ion association in concentrated solutions of electrolytes at physical temperatures, at non-polarity solvents or at low temperatures³⁴. The dissociation constant K_d of a chemical reaction is an experimentally measurable observable whose value can indicate the chemical state of the solution. If the initial reactant concentrations are lower than K_d , most of the ion pairs are expected to be in the dissolved state which will result in screening of the polyampholyte’s electrostatic interactions. On the other hand, when the reactant concentrations are considerably higher than K_d , most of the ion pairs are expected to be in the charge-neutral complex state which will affect the configuration entropy of the polyampholyte by modulating the effective excluded volume through steric repulsion. In addition, ion-pair association is often accompanied by a change in volume^{35–37}. Any such volume change might have an important effect—in addition to the electrostatic screening effects of the ions—on polyampholyte conformation at high reactant concentrations. Thus, the chemical state of the solution determined by Eq. (1) has potential to dictate LLPS behavior of the polyampholyte species.

At high salt concentrations, non-electrostatic interactions are expected to play a major role in determining LLPS behavior. Indeed, in a recent explicit chain molecular dynamics (MD) study, phase separation behaviour of several proteins at high salt concentrations were attributed to non-electrostatic interactions such as hydrophobic interactions²⁸. In a different study, the importance of the excluded volume interaction from PEG crowding agents was highlighted in a system with a phase separating protein that lack hydrophobic amino acids in its sequence³⁸. A model that includes both ion-association along with any volume change upon ion association and explicit residue level electrostatics of the phase separating polyampholyte thus offers a unique possibility of capturing many of the diverse results mentioned above in an unified set-up, at least qualitatively.

With that in mind, here we adopt a trade-off between complexity and analytical/computational tractability by introducing a simple field theory model where molecular species in the model interact via excluded volume and explicit sequence dependent electrostatic interactions. Specifically, we introduce a bare dissociation constant (corresponding to the dissociation constant in a solution consisting only of A^+ , B^- , and AB) as a control parameter for the non-electrostatic energy gain associated with ion-pairing. To account for the volume change upon association, we introduce further a relative excluded vol-

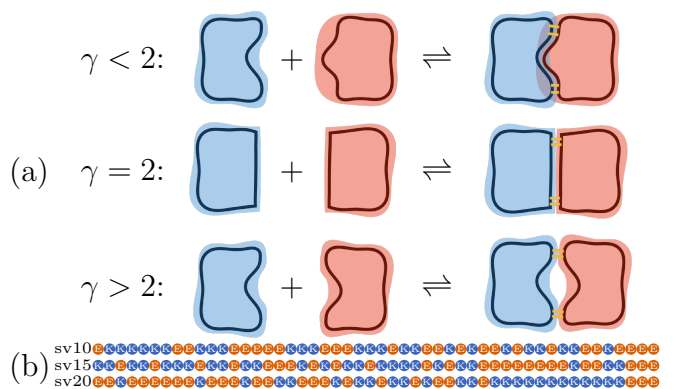


FIG. 1. (a) Schematic illustration of the effective volume change upon ion-association, modeled by the parameter γ . The shading represents volumetric effect beyond that of the van der Waals volume represented by the solid outlines of the solutes. (b) Charge sequences considered in this work. Blue (‘K’) and red (‘E’) beads correspond to charges $+1$ and -1 , respectively.

ume factor γ of the product AB in Eq. (1) with respect to the reactants A and B . We study the model using MFT, random phase approximation (RPA)—where relevant Gaussian level fluctuations are included above the MFT³⁹, and fully fluctuating field theoretic simulation (FTS). We expect the model to be useful as a base for studying specific systems with suitable modifications.

The structure of this article is as follows. In Sec. II, we introduce our model and derive its corresponding field theory representation in Sec. II A. The model is studied analytically in Sec. III using MFT and RPA, and then using FTS in Sec. IV. Numerical results obtained from the approximate analytical calculations and from FTS are shown and compared in Sec. V, and concluding remarks are given in Sec. VI.

II. MODEL DEFINITION

Our system of consideration contains n_p linear polymers of identical composition, each consisting of N residues with electric charges σ_α , $\alpha = 1, \dots, N$. Effects from solvent molecules are assumed to be implicitly encoded in the microscopic interaction parameters. All electric charges in this work are given in units of the elementary protonic charge, and we restrict our calculations to polymers with zero net electric charge, $\sum_{\alpha=1}^N \sigma_\alpha = 0$. The ‘K’-‘E’ sequences (Fig. 1 (b)) considered here are representative of the ‘sv sequences’⁴⁰ used extensively to study LLPS in computational models^{18,19,21,41–43}. An analytically derived single chain property, the sequence charge decoration (SCD) parameter (defined as $SCD = \sum_{\beta=2}^N \sum_{\alpha=1}^{\beta-1} \sigma_\beta \sigma_\alpha \sqrt{(\beta - \alpha)/N}$), could be used to discriminate between otherwise charge neutral ‘sv’ sequences⁴⁴. The phase separation propensity trends

of the “sv sequences” is known to correlate well with their SCD parameter values^{19,21,41}. A ‘K’-‘E’ sequence ((K₈E₈)₃) with SCD value -4.290 has recently been seen to be phase separating in an *in vitro* experiment⁴⁵. Compared to that the SCD values of the sequences studied here are -2.098, -4.349 and -7.374, respectively for sv10, sv15 and sv20. However, we emphasize that the model presented here is not intended to be quantitatively accurate given that we ignore some effects that are present in experimental systems, e.g. the possibility of ion condensation onto the polymer residues due to attractive interactions beyond the simple Coulomb forces^{45–50}. Consequently, while the trend predicted by our theory is expected to hold for corresponding experimental results, there are uncertainties^{43,51} in mapping the theoretical variables such as temperature to their experimental counterparts for individual systems.

The system further contains equal amounts of unit positive and negative model ions (denoted A⁺ and B⁻, respectively) that can undergo a pair-wise chemical reaction forming a neutral complex AB according to Eq. (1). The number of A/B pairs in the dissociated and bound state, n_A ($= n_B$) and n_{AB} respectively, are thus constrained according to

$$n_A + n_{AB} = n_T, \quad (3)$$

where n_T denotes the total number of A and B units in the system.

The position of bead α on polymer $i = 1, \dots, n_p$ is denoted $\mathbf{R}_{i,\alpha}$, while the positions of the A⁺, B⁻ and AB particles are represented by $\{\mathbf{r}_{A,i}\}_{i=1}^{n_A}$, $\{\mathbf{r}_{B,i}\}_{i=1}^{n_B}$ and $\{\mathbf{r}_{AB,i}\}_{i=1}^{n_{AB}}$, respectively. Quantities that depend explicitly on molecule positions are indicated by a hat (e.g. \hat{H}). All energies in this work are given in units of the thermal energy $k_B T$. The total Hamiltonian is $\hat{H} = \hat{H}_0 + \hat{H}_1 + \hat{H}_2 + \hat{H}_3$, where

$$\begin{aligned} \hat{H}_0 &= \frac{3}{2b^2} \sum_{i=1}^{n_p} \sum_{\alpha=1}^{N-1} (\mathbf{R}_{i,\alpha+1} - \mathbf{R}_{i,\alpha})^2, \\ \hat{H}_1 &= \frac{v}{2} \int d\mathbf{r} \hat{\rho}(\mathbf{r}), \\ \hat{H}_2 &= \frac{l_B}{2} \int d\mathbf{r} \int d\mathbf{r}' \frac{\hat{c}(\mathbf{r})\hat{c}(\mathbf{r}')}{|\mathbf{r} - \mathbf{r}'|}. \end{aligned} \quad (4)$$

These terms provide, respectively, the energies associated with harmonic chain connectivity, excluded volume repulsion, and electrostatic interactions. Here b is the polymer segment length, v is the excluded volume parameter and $l_B = e^2/4\pi\epsilon k_B T$ is the Bjerrum length (v and l_B modulate the strengths of the excluded volume- and electrostatic interactions, respectively). We use the segment length b as our unit of length, and thus values of all dimensionfull quantities (those that carry a physical unit) are given in powers of b . We have expressed $\hat{H}_{1,2}$ in terms of the microscopic particle densities and charge

densities, defined respectively as

$$\hat{\rho}(\mathbf{r}) = \hat{\rho}_b(\mathbf{r}) + \hat{\rho}_A(\mathbf{r}) + \hat{\rho}_B(\mathbf{r}) + \gamma \hat{\rho}_{AB}(\mathbf{r}), \quad (5)$$

$$\hat{c}(\mathbf{r}) = \hat{c}_b(\mathbf{r}) + \hat{\rho}_A(\mathbf{r}) - \hat{\rho}_B(\mathbf{r}), \quad (6)$$

where $\hat{\rho}_b(\mathbf{r}) = \sum_{i,\alpha} \Gamma(\mathbf{r} - \mathbf{R}_{i,\alpha})$, $\hat{c}_b(\mathbf{r}) = \sum_{i,\alpha} \sigma_\alpha \Gamma(\mathbf{r} - \mathbf{R}_{i,\alpha})$, $\hat{\rho}_j(\mathbf{r}) = \sum_i \Gamma(\mathbf{r} - \mathbf{r}_{j,i})$ for $j = A, B, AB$ and γ represents the relative excluded volume strength of the AB complex to a free ion (either A⁺ or B⁻). Individual polymer beads and ions are treated as Gaussian distributions $\Gamma(\mathbf{r}) = e^{-r^2/2a^2}/(2\pi a^2)^{3/2}$ with smearing length $a = b/\sqrt{6}$ to regulate ultraviolet divergences arising from contact excluded volume- and electrostatic contact interactions^{52,53}. This Gaussian smearing procedure has also been shown to remedy unphysical binding behaviour in models of highly concentrated polyelectrolyte solutions that combine equilibrium constants with Debye-Hückel treatment of electrostatic interactions⁴⁷. In this work, we view the Gaussian smearing as a part of the model definition, rather than as an approximation. While leaving the long-range behavior of inter-particle forces unaffected, the Gaussian smearing results in short-range interactions that are considerably “softer” than typical hard-sphere or Lennard-Jones particle representations⁴². Consequently, the model is not expected to capture microscopic phenomena such as strongly oscillating radial distribution functions on short distance scales that typically characterizes liquid phases⁵⁴.

The parameter γ in Eq. (5) may be interpreted through the effective volume of the AB state relative to its dissociated counterpart, with the sign of $\gamma - 2$ corresponding to the sign of $\text{vol}(AB) - \text{vol}(A^+) - \text{vol}(B^-)$ as illustrated schematically in Fig. 1 (a). The resulting AB-AB and AB-[other monomer = A⁺, B⁻, (polymer bead)] excluded volume interaction strengths are scaled as γ^2 and γ , respectively, relative to the [other monomer]-[other monomer] excluded volume repulsion strength v . At the MFT level of an analogous model that takes the AB bound state as an independent system component, these excluded volume interactions result in effective χ -parameters that are scaled by the same powers of γ , and our framework is therefore related to other approaches in the literature^{55–57} where effective ion size effects are modeled through appropriate χ -parameter variations. Implications of effective ion sizes on counter-ion condensation have also been considered within the context of polyelectrolyte complex coacervation⁴⁸.

The final piece of the Hamiltonian, \hat{H}_3 , models the chemical binding of the AB complex,

$$\hat{H}_3 = (n_T - n_{AB})\epsilon_{\text{bound}}, \quad (7)$$

where $-\epsilon_{\text{bound}}$ is the decrement in free energy associated with a single AB binding, in addition to electrostatic and excluded volume contributions coming from $\hat{H}_{1,2}$. Note that ϵ_{bound} may include both an energetic component, as well as an entropic component related e.g. to changes in the number of configuration states, or the entropy release from reduced electrostriction of nearby solvent

molecules⁵⁸. In the remainder of this article, we find it convenient to trade ϵ_{bound} in favor of another parameter K_0 , defined as

$$K_0 = \frac{e^{-\epsilon_{\text{bound}}}}{\lambda_{\text{th}}^3}, \quad (8)$$

where λ_{th} is the thermal de Broglie wavelength. We show in Sec. III A that K_0 corresponds to the mean-field dissociation constant in the dilute limit. This simple physical interpretation of K_0 breaks down when particle and charge fluctuations are taken into consideration, as shown in Sec. III B.

The partition function of the system,

$$Z = \sum_{n_{\text{AB}}=0}^{n_{\text{T}}} \frac{\int \{d\mathbf{R}\} \{d\mathbf{r}_A\} \{d\mathbf{r}_B\} \{d\mathbf{r}_{\text{AB}}\} e^{-\hat{H}}}{\tilde{V}^{-(n_{\text{p}}+2n_{\text{A}}+n_{\text{AB}})} n_{\text{p}}! (n_{\text{A}}!)^2 n_{\text{AB}}!}, \quad (9)$$

is expressed as a sum over the number paired ions n_{AB} , where n_{A} is constrained to $n_{\text{T}} - n_{\text{AB}}$ according to Eq. (3) and $\tilde{V} = V/\lambda_{\text{th}}^3$. In Eq. (9), we use a short-hand notation $\{d\mathbf{R}\} \equiv \prod_{i=1}^{n_{\text{p}}} \prod_{\alpha=1}^N d\mathbf{R}_{i,\alpha}$ and $\{d\mathbf{r}_j\} \equiv \prod_{i=1}^{n_j} d\mathbf{r}_{j,i}$ (for $j = \text{A, B, AB}$) to indicate that the integrals are performed over the positions of all polymer beads, solvated ions and bound ion pairs. The factorials in the denominator follow from the fact that the polymers and the A^+ , B^- and AB solute are separately indistinguishable. Note that the particular combination $(n_{\text{A}}!)^2 n_{\text{AB}}!$ implies that a bound state AB is distinguishable from any configuration of a free A^+/B^- pair.

The logarithm of the partition function in Eq. (9) can be used to define a free energy density $f(\rho_{\text{b}}, \rho_{\text{T}}; K_0, l_{\text{B}}, v, \dots) = -(\ln Z)/V$, where V is the system volume, $\rho_{\text{b}} = n_{\text{p}}N/V$ is the bulk polymer bead number density and $\rho_{\text{T}} = n_{\text{T}}/V$ is the total bulk number density of A and B ions. We can compute the average number density of solvated ions $[\text{A}^+] = [\text{B}^-] = \langle n_{\text{A}} \rangle / V$ through the first derivative of f with respect to K_0 ,

$$[\text{A}^+] = -K_0 \frac{\partial f}{\partial K_0}. \quad (10)$$

The constraint (3) then gives average number density of bound ion pairs as $[\text{AB}] = \rho_{\text{T}} - [\text{A}^+]$. Knowledge of $[\text{A}^+]$ and $[\text{AB}]$ can subsequently be used to compute the dissociation constant K_{d} according to Eq. (2). Other thermodynamic quantities of interest to this work are the polymer chain- and ion pair chemical potentials, $\mu_{\text{p}} = N\partial f/\partial \rho_{\text{b}}$ and $\mu_{\text{T}} = \partial f/\partial \rho_{\text{T}}$ respectively, and the osmotic pressure $\Pi = \rho_{\text{b}}\mu_{\text{p}}/N + \rho_{\text{T}}\mu_{\text{T}} - f$.

Note that K_{d} in Eq. (2) in principle depends on how the bound state concentration $[\text{AB}]$ is defined. In this work, we consider the contributing AB states as chemically distinct (e.g. through the appearance of a covalent bond between A and B , an ionic bond between A^+ and B^- with strength beyond that of simple electrostatic attraction, or some other mechanism) from any configuration of free A^+ and B^- molecules, as follows from the relation in Eq. (10) combined with the factorials in the

denominator in Eq. (9). If $[\text{AB}]$ is measured by exploiting the electrostatic properties of the A^+-B^- solution, rather than the chemical nature of the AB bond, a different definition of $[\text{AB}]$ might be more appropriate where nearby A^+ and B^- molecules are counted as effectively bound. This would be better captured by defining $[\text{A}^+]$ and $[\text{B}^-]$ through their corresponding activity parameters, similarly to how pH is formally defined through proton activity parameter rather than concentration⁵⁹. For simplicity, this alternative approach is not pursued further in this work.

A. Deriving the field theory

The basis of the analytical calculations and lattice simulations is a field representation of the partition function in Eq. (9). To derive its corresponding field theory, we first decouple the interaction terms in \hat{H}_1 and \hat{H}_2 through standard Hubbard-Stratonovich transformations^{60,61}. This introduces two fields $w(\mathbf{r})$ and $\psi(\mathbf{r})$, conjugate to $\hat{\rho}(\mathbf{r})$ and $\hat{c}(\mathbf{r})$, respectively, and leads to

$$Z = \frac{\int \mathcal{D}w \int \mathcal{D}\psi Q_{\text{p}}^{n_{\text{p}}} (Q_{\text{A}}Q_{\text{B}})^{n_{\text{T}}} e^{-H_0[w,\psi]} S[w,\psi]}{n_{\text{p}}! V^{-2n_{\text{T}}} \lambda_{\text{th}}^{3n_{\text{T}}} K_0^{-n_{\text{T}}} Z_w Z_{\psi}}. \quad (11)$$

up to an inconsequential multiplicative constant, where $H_0[w,\psi] = \int d\mathbf{r} [w^2/2v + (\nabla\psi)^2/8\pi l_{\text{B}}]$. The factor $S[w,\psi]$ contains the sum over n_{AB} ,

$$S = \sum_{n_{\text{AB}}=0}^{n_{\text{T}}} \frac{1}{n_{\text{AB}}! [(n_{\text{T}} - n_{\text{AB}})!]^2} \left(\frac{V^{-1} Q_{\text{AB}}}{K_0 Q_{\text{A}} Q_{\text{B}}} \right)^{n_{\text{AB}}}. \quad (12)$$

In the above expressions, $Q_i \equiv Q_i[w(\mathbf{r}), \psi(\mathbf{r})]$ for $i = \text{p, A, B, AB}$ is the partition function for a type i molecule in presence of chemical- and electrostatic potential fields $i\check{w}(\mathbf{r}) \equiv \Gamma \star iw(\mathbf{r})$ and $i\check{\psi}(\mathbf{r}) \equiv \Gamma \star i\psi(\mathbf{r})$ (where \star denotes spatial convolution, i.e. $\Gamma \star \phi(\mathbf{r}) \equiv \int d\mathbf{r}' \Gamma(\mathbf{r}-\mathbf{r}') \phi(\mathbf{r}')$ for any function $\phi(\mathbf{r})$). For our model components, we have

$$Q_{\text{p}} = \int d\mathbf{R}_{1,\dots,N} \frac{e^{-\frac{3}{2b^2} \sum_{\alpha=1}^{N-1} \Delta \mathbf{R}_{\alpha}^2 - \sum_{\alpha=1}^N i\check{W}_{\alpha}}}{V(2\pi b^2/3)^{3(N-1)/2}}, \quad (13)$$

where $\Delta \mathbf{R}_{\alpha} \equiv \mathbf{R}_{\alpha+1} - \mathbf{R}_{\alpha}$, $\check{W}_{\alpha} \equiv \check{w}(\mathbf{R}_{\alpha}) + \sigma_{\alpha} \check{\psi}(\mathbf{R}_{\alpha})$, and

$$Q_{\text{AB}} = \frac{1}{V} \int d\mathbf{r} e^{-\gamma i\check{w}(\mathbf{r})}, \quad Q_{\text{A}} = \frac{1}{V} \int d\mathbf{r} e^{-i[\check{w}(\mathbf{r}) + \check{\psi}(\mathbf{r})]},$$

and,

$$Q_{\text{B}} = \frac{1}{V} \int d\mathbf{r} e^{-i[\check{w}(\mathbf{r}) - \check{\psi}(\mathbf{r})]}. \quad (14)$$

Note that all Q_i are normalized to $Q_i[0,0] = 1$. The factors $Z_w \equiv \int \mathcal{D}w \exp(-\int d\mathbf{r} w^2/2v)$ and $Z_{\psi} \equiv \int \mathcal{D}\psi \exp(-\int d\mathbf{r} (\nabla\psi)^2/8\pi l_{\text{B}})$ have been inserted to provide additive density-independent contributions to the osmotic pressure that cancels the divergent contributions

of the $|\mathbf{k}| > a^{-1}$ modes of the functional integrals in Eq. (11)^{43,62}.

In the thermodynamic limit, the sum over n_{AB} in S may be replaced by an integral that can be solved in the saddle-point approximation (this step is shown in Appendix A). The resulting field picture representation of the partition function becomes

$$Z = \frac{\tilde{V}^{n_p+n_T} \int \mathcal{D}w \int \mathcal{D}\psi e^{-H[w,\psi]}}{n_p!n_T! Z_w Z_\psi}, \quad (15)$$

where the field Hamiltonian is

$$H[w, \psi] = H_0 - n_p \ln Q_p - n_T \ln Q_{AB} + n_T h_0(x). \quad (16)$$

Here, we have introduced a field operator $x[w, \psi]$,

$$x[w, \psi] \equiv \frac{2\rho_T}{K_0} \frac{Q_{AB}}{Q_A Q_B} \quad (17)$$

and the function

$$h_0(x) = \ln \left(1 - \frac{\sqrt{1+2x}-1}{x} \right) - \frac{\sqrt{1+2x}-1}{x}. \quad (18)$$

In the following, we find it useful to define two additional functions, $h_1(x) \equiv x h'_0(x)$ and $h_2(x) \equiv x h'_1(x)$, where in particular

$$h_1(x) = \frac{\sqrt{1+2x}-1}{x}, \quad (19)$$

satisfies $0 \leq h_1(x) \leq 1$ for any real $x \geq 0$ (similarly, it may be shown that $h_2(x) \leq 0$). The physical interpretation of the field operator $h_1(x[w, \psi])$ becomes clear when applying the relation in Eq. (10) to the field partition function in Eq. (15), leading to

$$[A^+] = \langle h_1(x) \rangle \rho_T, \quad (20)$$

i.e. $h_1(x[w, \psi])$ is a field operator that averages to the fraction of dissociated A/B pairs. Correspondingly, $[AB] = \rho_T [1 - \langle h_1(x) \rangle]$ gives the number density of the bound ion species. The field averaged $h_1(x[w, \psi])$ can therefore be used to evaluate K_d in Eq. (2),

$$K_d = \rho_T \frac{\langle h_1 \rangle^2}{1 - \langle h_1 \rangle}. \quad (21)$$

III. ANALYTICAL THEORY

To understand the physical implications of our model in Eq. (9), we now proceed to approximately evaluate the functional integrals in the field representation of the partition function in Eq. (15). The mean field theory (MFT) solution, which only accounts for the spatially homogeneous field configurations, captures the dominant effects on ion dissociation from excluded volume interactions and, in particular, showcases the crucial role of the

parameter γ . However, effects from electrostatic interactions are entirely given by fluctuations of the charge-conjugate field $\psi(\mathbf{r})$, which are not accounted for in MFT³³. To capture the leading-order electrostatic effects, we next evaluate Eq. (15) in the random phase approximation (RPA). This accounts for Gaussian field fluctuations described by the expansion of $H[w, \psi]$ truncated beyond quadratic order in $w(\mathbf{r})$ and $\psi(\mathbf{r})$ (corresponding to fluctuations in density and charge, respectively).

A. Mean field theory

A spatially homogeneous $\psi(\mathbf{r}) = \bar{\psi}$ does not contribute in the field Hamiltonian in Eq. (16) due to the over-all charge neutrality of the system, and hence does not contribute in MFT. The MFT solution for $w(\mathbf{r}) = \bar{w}$, given by the vanishing first derivative of $H[w, 0]$, satisfies

$$i\bar{w} = v\bar{\rho}_{\text{tot}}, \quad (22)$$

where

$$\bar{\rho}_{\text{tot}} = \rho_b + [2\bar{h}_1 + \gamma(1 - \bar{h}_1)] \rho_T \quad (23)$$

is the total concentration in MFT (counting each AB complex as γ units), and $\bar{h}_1 \equiv h_1(x[\bar{w}, 0])$ with $x[\bar{w}, 0] = 2\rho_T e^{(2-\gamma)i\bar{w}}/K_0$. The exponential dependence of \bar{h}_1 on \bar{w} means that Eq. (22) generally lacks a closed-form solution, except for in the special case when $\gamma = 2$, and therefore has to be solved numerically for each given set of parameter values.

Setting $\langle h_1 \rangle = \bar{h}_1$ in Eq. (21) gives the MFT expression for the dissociation constant, which may be simplified to

$$\bar{K}_d = K_0 \exp[(\gamma - 2)v\bar{\rho}_{\text{tot}}]. \quad (24)$$

In the dilute limit, $\rho_b, \rho_T \rightarrow 0$, this expression reduces to $\bar{K}_d = K_0$ verifying the claim in the previous section that the parameter K_0 is the dilute-limit MFT dissociation constant. In the opposite limit, where either ρ_b or ρ_T are large, the dissociation constant instead either becomes exponentially suppressed (for $\gamma < 2$) or exponentially enhanced (for $\gamma > 2$) at densities $\gtrsim (|\gamma - 2|v)^{-1}$. Physically, this may be interpreted as the bound AB state being either favored or disfavored in a dense system depending on if it yields favorable excluded volume interactions compared to the dissociated state A^+/B^- . At $\gamma = 2$, the MFT dissociation constant is density independent.

The MFT evaluation of the functional integrals $Z_w^{-1} Z_\psi^{-1} \int \mathcal{D}w \int \mathcal{D}\psi \exp(-H[w, \psi]) \approx \exp(-H[\bar{w}, 0])$ leads to the following expression for the free energy density,

$$\bar{f} = -s_0 + \rho_T \bar{h}_0 + \frac{v}{2} \bar{\rho}_{\text{tot}} [\bar{\rho}_{\text{tot}} - 2(2 - \gamma)\bar{h}_1 \rho_T],$$

where $\bar{h}_0 \equiv h_0(x[\bar{w}, 0])$, and

$$s_0 = \frac{1}{V} \ln \frac{V^{n_p+n_T}}{n_p!n_T!},$$

is the configuration entropy density for a system with fully associated ions. The MFT chemical potentials and osmotic pressure that follow are

$$\begin{aligned}\bar{\mu}_p &= \ln \frac{\rho_b}{N} + vN\bar{\rho}_{\text{tot}}, \\ \bar{\mu}_T &= \ln [\rho_T(1 - \bar{h}_1)] + v\gamma\bar{\rho}_{\text{tot}}, \\ \bar{\Pi} &= \frac{\rho_b}{N} + (1 + \bar{h}_1)\rho_T + \frac{v}{2}\bar{\rho}_{\text{tot}}^2.\end{aligned}$$

B. Gaussian fluctuations: random phase approximation

The Gaussian field fluctuations can be accounted for by expanding the field Hamiltonian $H[w, \psi]$ in Eq. (16) to quadratic order about the MFT solution, and then performing the resulting Gaussian functional integrals in the partition function. This leads to the following correction term to the free energy density,

$$f = \bar{f} + \frac{1}{2} \int \frac{d\mathbf{k}}{(2\pi)^3} \ln \left[\frac{4\pi l_B v}{\mathbf{k}^2} \det \mathbf{G}(\mathbf{k}) \right], \quad (25)$$

where $\mathbf{G}(\mathbf{k})$ is the 2-by-2 matrix with the Fourier representation of the coefficients of the quadratic terms in the expansion of $H[w, \psi]$ and the factor $4\pi l_B v / \mathbf{k}^2$ comes from the product $Z_w Z_\psi$ in the denominator of Eq. (15). Using the field basis (w, ψ) , we may write

$$\mathbf{G}(\mathbf{k}) = \mathbf{G}_0(\mathbf{k}) + \rho_b \mathbf{G}_p(\mathbf{k}) + \rho_T \mathbf{G}_T(\mathbf{k}),$$

where $\mathbf{G}_0(\mathbf{k}) = \text{diag}(1/v, \mathbf{k}^2/4\pi l_B)$, $\mathbf{G}_T(\mathbf{0}) = \text{diag}(-(2 - \gamma)^2 \bar{h}_2, 0)$, $\mathbf{G}_T(\mathbf{k} \neq \mathbf{0}) = \hat{\Gamma}(\mathbf{k})^2 \text{diag}(\gamma^2 + (2 - \gamma^2)\bar{h}_1, 2\bar{h}_1)$, $\mathbf{G}_p(\mathbf{0}) = \text{diag}(0, 0)$ and

$$\mathbf{G}_p(\mathbf{k} \neq \mathbf{0}) = \hat{\Gamma}(\mathbf{k})^2 \begin{pmatrix} g_{mm}(\mathbf{k}) & g_{mc}(\mathbf{k}) \\ g_{mc}(\mathbf{k}) & g_{cc}(\mathbf{k}) \end{pmatrix}.$$

The entries of $\mathbf{G}_p(\mathbf{k} \neq \mathbf{0})$ are the standard single chain density-density-, density-charge- and charge-charge correlations following from the expansion of Q_p , i.e. $g_{mm}(\mathbf{k}) = \sum_{\alpha, \beta=1}^N e^{-|\alpha - \beta|b^2 \mathbf{k}^2/6}/N$, $g_{mc}(\mathbf{k}) = \sum_{\alpha, \beta=1}^N \sigma_\alpha e^{-|\alpha - \beta|b^2 \mathbf{k}^2/6}/N$ and $g_{cc}(\mathbf{k}) = \sum_{\alpha, \beta=1}^N \sigma_\alpha \sigma_\beta e^{-|\alpha - \beta|b^2 \mathbf{k}^2/6}/N$. In the above expressions, $\hat{\Gamma}(\mathbf{k}) = e^{-a^2 \mathbf{k}^2/2}$ is the Fourier transformation of the Gaussian smearing function $\Gamma(\mathbf{r})$.

The derivatives of Eq. (25) with respect to species numbers, volume and K_0 yields corrections from Gaussian field fluctuations to the chemical potentials, osmotic pressure and fraction of dissociated ion pairs, $\mu_p = \bar{\mu}_p + \mu_p^{(\text{fl})}$, $\mu_p = \bar{\mu}_p + \mu_p^{(\text{fl})}$, $\mu_T = \bar{\mu}_T + \mu_T^{(\text{fl})}$, $\Pi = \bar{\Pi} + \Pi^{(\text{fl})}$ and $\langle h_1(x) \rangle = \bar{h}_1 + h_1^{(\text{fl})}$, respectively. The full expressions for the RPA corrections $X^{(\text{fl})}$ are given in Appendix B.

The RPA contributions to our thermodynamic observables of interest all involve integrals over wave numbers \mathbf{k} that generally need to be computed numerically. A special case, that can be treated fully analytically, is the

dilute limit of $h_1^{(\text{fl})}$, leading to the following RPA expression for the dilute limit dissociation constant,

$$\lim_{\rho_b, \rho_T \rightarrow 0} K_d = K_0 \left(1 + \frac{(2 - \gamma^2)v}{16\pi^3/2a^3} + \frac{l_B}{\sqrt{\pi}a} \right)^{-1}. \quad (26)$$

This shows that the bare parameter K_0 can no longer be interpreted as the dilute limit dissociation constant when fluctuations are included in the calculation.

IV. FIELD THEORY SIMULATIONS

We complement our findings from RPA calculations with field theoretical simulations (FTS) that fully capture the fluctuations of the fields $w(\mathbf{r})$ and $\psi(\mathbf{r})$. Other alternative simulation approaches to biomolecular LLPS include explicit chain MD simulations^{18,41,63,64} and finite-size scaling theory^{65,66}. In FTS, equilibrium evolution of the system dictated by the Hamiltonian Eq. (16) is studied by following a complex Langevin (CL) prescription^{61,67-71} where the real-valued continuous fields w and ψ are analytically continued to their respective complex planes and evolved in the fictitious CL time through the equations given by

$$\begin{aligned}\frac{\partial w(\mathbf{r}, t)}{\partial t} &= - \left[i\tilde{\rho}(\mathbf{r}, t) + \frac{w(\mathbf{r}, t)}{v} \right] + \eta_w(\mathbf{r}, t), \\ \frac{\partial \psi(\mathbf{r}, t)}{\partial t} &= - \left[i\tilde{c}(\mathbf{r}, t) - \frac{\nabla^2 \psi(\mathbf{r}, t)}{4\pi l_B} \right] + \eta_\psi(\mathbf{r}, t).\end{aligned} \quad (27)$$

This allows ensemble averages to be computed as asymptotic CL time averages. In Eq. (27), η_w and η_ψ are real valued random numbers with zero mean and variance $2\delta(\mathbf{r} - \mathbf{r}')\delta(t - t')$. The field operators for the number- and charge densities, $\tilde{\rho} \equiv \tilde{\rho}_b + \tilde{\rho}_A + \tilde{\rho}_B + \tilde{\rho}_{AB}$ and $\tilde{c} \equiv \tilde{c}_b + \tilde{\rho}_A - \tilde{\rho}_B$, respectively, are obtained from

$$\tilde{\rho}_b(\mathbf{r}, t) = in_p \frac{\delta \ln Q_p}{\delta w(\mathbf{r}, t)}, \quad \text{and} \quad \tilde{c}_b(\mathbf{r}, t) = in_p \frac{\delta \ln Q_p}{\delta \psi(\mathbf{r}, t)}, \quad (28)$$

for polymers, and

$$\begin{aligned}\tilde{\rho}_i(\mathbf{r}, t) &= h_1(x) in_T \frac{\delta \ln Q_i}{\delta w(\mathbf{r}, t)}, \quad i = A, B, \\ \tilde{\rho}_{AB}(\mathbf{r}, t) &= [1 - h_1(x)] in_T \frac{\delta \ln Q_{AB}}{\delta w(\mathbf{r}, t)},\end{aligned} \quad (29)$$

for ions where $x[w, \psi]$ is defined in Eq. (17). Detailed expressions for the above density operators can be found in Appendix C. Note that contributions from field fluctuations up to all orders are kept in Eqs. (28) and (29). We numerically solve Eq. (27) on a cubic lattice with periodic boundary conditions and lattice spacing Δx , using a semi-implicit first order time stepping method^{43,72} with a CL time-step $\Delta t = 10^{-3}b^3$. Use of the semi-implicit time stepping method results in significantly better numerical stability compared to the Euler-Maruyama type explicit

time-discretization methods⁷². As with the CL-time discretization, the spatial discretization of the continuous fields w and ψ is an approximation, and, formally, FTS only exactly reproduces the continuum field theory in the limit $\Delta x \rightarrow 0$. However, the Gaussian smearing already provides a strong exponential suppression of contributions from field fluctuations on distance scales smaller than the smearing length a , such that these modes may be omitted with a negligible numerical effect on physical observables. In this work, we therefore set $\Delta x = a$ in all FTS computations.

Thermally averaged bulk densities of solvated and bound ion concentrations can be obtained from the field

$$g_{p,p}(|\mathbf{r} - \mathbf{r}'|) = \frac{1}{\rho_b \rho'_b} \left[\frac{i}{v} \langle \tilde{\rho}_b(\mathbf{r}) w(\mathbf{r}') \rangle - \sum_i \langle \tilde{\rho}_b(\mathbf{r}) \tilde{\rho}_i(\mathbf{r}') \rangle \right] - \frac{1}{\rho'_b} \frac{e^{-(\mathbf{r}-\mathbf{r}')^2/4a^2}}{(4\pi a^2)^{3/2}}, \quad i = A, B, AB, \quad (31)$$

$$g_{p,S}(|\mathbf{r} - \mathbf{r}'|) = \frac{\langle \tilde{\rho}_b(\mathbf{r}) [\tilde{\rho}_A(\mathbf{r}') + \tilde{\rho}_B(\mathbf{r}')] \rangle}{2\rho_b \rho_T \langle h_1 \rangle}, \quad \text{and,} \quad g_{p,B}(|\mathbf{r} - \mathbf{r}'|) = \frac{\langle \tilde{\rho}_b(\mathbf{r}) \tilde{\rho}_{AB}(\mathbf{r}') \rangle}{\gamma \rho_b \rho_T (1 - \langle h_1 \rangle)},$$

where the subscripts p, S and B on the RDFs stand for polymer bead, solvated and bound, respectively. The last term in the expression for $g_{p,p}(r)$ subtracts the contribution from the polymer bead with itself. The RDFs in Eq. (31) have been normalized to $g_{i,j} = 1$ when units of i and j are uncorrelated, which is expected e.g. at large r if the system contains a single liquid phase. In Eq. (31), the factor $\rho'_b = \rho_b - N/V$ provides the correct finite-volume correction to the polyampholyte–polyampholyte RDF normalisation, and approaches ρ_b at large V .

If the system is in a globally inhomogeneous state, e.g. by containing several co-existing macro-phases, certain PMFs may approach non-zero values at large separations r . In particular, the large r behavior of the polyampholyte–polyampholyte PMF $U_{p,p}(r)$ indicates if the polymers are homogeneously distributed on large scales or are concentrated in e.g. a dense droplet. The information of the influences of the solvated ions and the neutral ion-pairs on phase separation, on the other hand, are obtained from the polyampholyte–solvated-ions and polyampholyte–ion-pair PMFs, respectively.

V. RESULTS

The effects on ion pairing from the solution condition can be understood from Fig. 2, showing K_d and $[A^+] = [B^-]$ computed in RPA and FTS as functions of ρ_T at $\gamma = 1.5, 2.0$ and 2.5 in polymer empty ($\rho_b = 0$) and dense ($\rho_b = 5b^{-3}$) systems with polyampholyte species sv15. The FTS calculations were done on a 32^3 lattice. The plots in Fig. 2 show excellent agreement between RPA and FTS except in the very dilute limit where

averaged value of $h_1(x)$. Information about how the components are spatially distributed in the system can be gleaned from potential of mean forces (PMFs). The PMF $U_{i,j}(r)$ between two components i and j describe the free-energy landscape for the separation r between two units of i and j , and is related to the corresponding radial distribution function (RDF) $g_{i,j}(r)$ through the relation

$$U_{i,j}(r) = -\ln g_{i,j}(r). \quad (30)$$

Here, $U_{i,j}(r)$ is given in units of the thermal energy $k_B T$. Since explicit particle coordinates have been traded off to the field degrees of freedom in the field picture, RDFs have to be computed through their field operators defined by⁴²

field fluctuations beyond Gaussian order are expected to become important. Proper sampling of important field configurations may not be possible through CL methods when the system is dictated by relatively high excluded volume interaction together with short range hydrophobicity type interactions⁷³. The agreement between the RPA and FTS results seen here is thus reassuring that Δt and Δx values used in the FTS implementation provide sufficient numerical accuracy. When the total density is $\lesssim (v|2 - \gamma|)^{-1}$, the dominant effect on the dissociation constant K_d comes from charges in the surroundings (either free ions or charged polymer residues) that screen out the electrostatic component of the A-B binding energy, thus increasing the value of K_d . In Fig. 2 (a), this effect underlies both the slow increase of K_d with increasing ρ_T at $\rho_b = 0$, and difference between the $\rho_b = 0$ and $\rho_b = 5b^3$ curves. At higher densities, where effects from excluded volume interactions instead dominate, the exponential dampening (for $\gamma < 2$) or enhancement (for $\gamma > 2$) of K_d determines whether mainly bound states AB, or free A^+ and B^- are present in the system, as can be seen in Fig. 2 (b).

Fig. 3 shows RPA phase diagrams for the system with sv15 polyampholyte species computed by matching the osmotic pressure $\Pi(\rho_b, \rho_T)$ and chemical potentials $\mu_p(\rho_b, \rho_T)$ and $\mu_T(\rho_b, \rho_T)$ along the phase boundary^{43,74}. The binodal curves (solid black curves) enclose the co-existence regions, where the co-existing bulk density values of ρ_b and ρ_T are connected by tie-lines (dashed lines). The background color gradient shows the density of solvated ions, $[A^+]$, expressed through

$$pA^+ \equiv -\log_{10}[A^+]b^3. \quad (32)$$

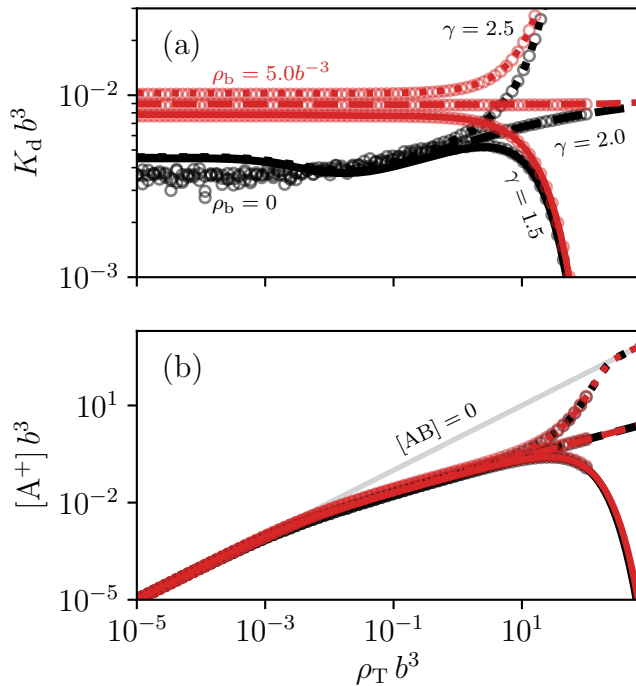


FIG. 2. The dissociation constant K_d (a) and solvated ion density $[A^+] = [B^-]$ (b) computed in RPA (curves) and FTS (circles) as functions of $\rho_T = [A^+] + [AB]$. Black and red correspond to systems with zero and high polymer density ($\rho_b = 0$ and $\rho_b = 5b^{-3}$), respectively. Values of γ are indicated by the linestyles with $\gamma = 1.5, 2$ and 2.5 corresponding to solid, dashed and dotted lines, respectively. The gray line in (b) indicates where all ions exist in the solvated state, i.e. $[A^+] = \rho_T$ and $[AB] = 0$. All results are computed using the sv15 charge sequence in Fig. 1(b) with $l_B = 0.6b$, $v = 0.05b^3$, $K_0 = 0.01b^{-3}$ and $a = b/\sqrt{6}$. The FTS results were computed on 32^3 cubic lattice with lattice spacing $\Delta x = b/\sqrt{6}$ and a Complex-Langevin time-step $\Delta t = 10^{-3}b^3$.

The phase diagrams in Fig. 3 display strong dependence on l_B and γ , and, in particular, predict the possibility of re-entrant phase separation with increasing ρ_T . A high ρ_T re-entrant phase separation region occurs at $l_B = 0.6b$ for $\gamma = 1.5$, but vanishes for $\gamma \geq 2$, which can be understood from the preferred ion-pairing state in the dense system. As can be seen from Fig. 2, for $\gamma = 1.5$, a large ρ_T strongly favors the charge neutral bound state AB which only interacts through excluded volume repulsion. The resulting crowding effects leads to an effective attraction between the chains that further promotes phase separation which enables the re-entrant phase separation. At $\gamma = 2.5$, the high ρ_T system contains almost exclusively solvated ions that strongly screen out the polymer electrostatic interactions, thus inhibiting phase separation. At the boundary value $\gamma = 2$, although the high ρ_T state still contains a substantial amount of bound ions, the small amount of solvated ions (behaving roughly as $[A^+] \sim \sqrt{\rho_T}$) is enough to dissolve the condensates.

When increasing l_B , the two disconnected co-existence regions at $\gamma = 1.5$, merge into one. Note that the considered polyampholyte species phase separates for both the l_B values used in Fig. 3 in the absence of any ions.

All tie-lines in Fig. 3 are roughly horizontal, but tend to have slightly positive and negative slopes (indicated by \uparrow 's and \downarrow 's) when the ions dominantly are solvated or exist in the bound state, respectively. This is exemplified in Fig. 4, where we show the tie-line slopes for the phase diagram in Fig. 3 (d) (i.e. at $l_B = 0.9b$ for $\gamma = 1.5$). The inset of Fig. 4 shows the region where the tie-line slopes change sign, beyond which the tie-line slope becomes increasingly more negative at higher ρ_T values.

In Fig. 5, we focus on the $\gamma = 1.5$ and $l_B = 0.6b$ phase diagram of Fig. 3 and investigate the dependence of the re-entrant phase behavior on the model parameters and the polymer charge sequence. The excluded volume parameter v plays different roles in the upper and lower regions of the re-entrance phase diagrams, as seen in Fig. 5 (a). While reducing the value of l_B (which reduces the strength of electrostatic interactions) or increasing K_0 (giving more solvated ions that provide electrostatic screening) both decrease the phase separation propensity by shrinking the two co-existence regions, a reduced v simultaneously enlarges the low ρ_T region and shrinks the high ρ_T region. The excluded volume interactions with AB molecules therefore act as to stabilize the high ρ_T condensates, while the excluded volume interactions among the polymers in the low ρ_T region inhibit phase separation. In Fig. 5 (b), we instead swap the sv15 charge sequence by either sv10 or sv20, which are characterized by smaller or larger blocks of consecutive same-sign charges, respectively. This degree of ‘‘blockiness’’ can be quantified e.g. by the κ parameter of Das and Pappu⁷⁵, or by the sequence charge decoration parameter of Sawle and Gosh⁴⁴, and has been shown to strongly correlate with phase separation propensity^{18,20,21,41,54}. Fig. 5 (b) shows that the phase diagram exhibits a strong dependence on the charge sequence blockiness, and that even the topology of the co-existence region may depend on the sequence (c.f. two disconnected co-existence regions of sv10 and sv15 versus the connected sv20 co-existence region).

We qualitatively verify some of the LLPS properties obtained from RPA calculations using FTS calculations of the PMFs $U_{p,p}(r)$, $U_{p,s}(r)$ and $U_{p,B}(r)$. For the PMF calculations, we now use a larger (48^3) lattice and focus on the polymer charge sequence sv15. Other fixed parameter values are $l_B = 0.6b^{-3}$, $v = 0.05b^3$, $K_0 = 0.01b^{-3}$ and $\rho_b = 0.1b^{-3}$. We simulate the system at various initial reactant concentrations and values of γ . The results for different ρ_T values are shown in Fig. 6. To obtain reliable statistics, we ran 5 independent simulations for each ρ_T . For each independent run, out of a total 1.5×10^5 CL time-steps, we discard the first 5×10^4 steps and use the rest to compute field averages of the RDFs using a sampling interval of 500 steps. The equilibration time was taken as the CL time step after which the real part

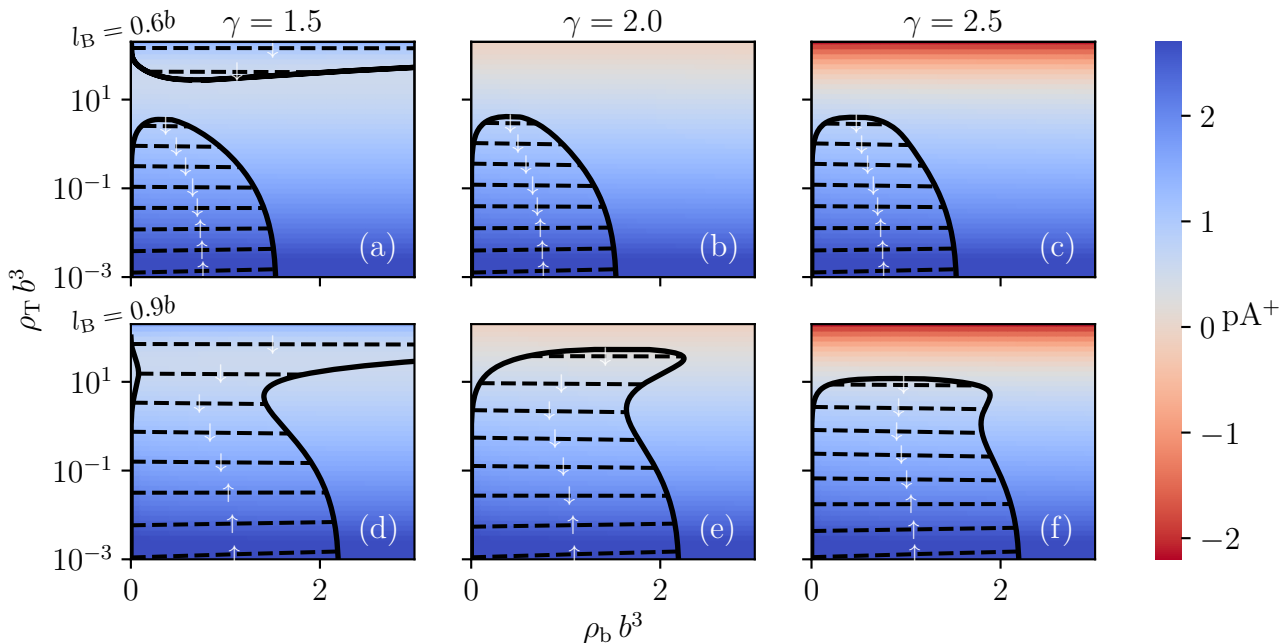


FIG. 3. RPA phase diagrams in the (ρ_b, ρ_T) plane. Sub-figures (a–c) in the top row correspond to $\gamma = 1.5, 2$ and 2.1 , respectively, and all with $l_B = 0.6b$. In the bottom row, sub-figures (d–f) are for a common $l_B = 0.9b$ and γ values $1.5, 2$ and 2.1 , respectively. Other parameter values are $v = 0.05b^3$, $K_0 = 0.01b^{-3}$ and $a = b/\sqrt{6}$. The color gradient shows the density of solvated ions $[A^+]$, expressed through Eq. (32). Tie-lines indicated by \uparrow and \downarrow have positive and negative slopes, respectively.

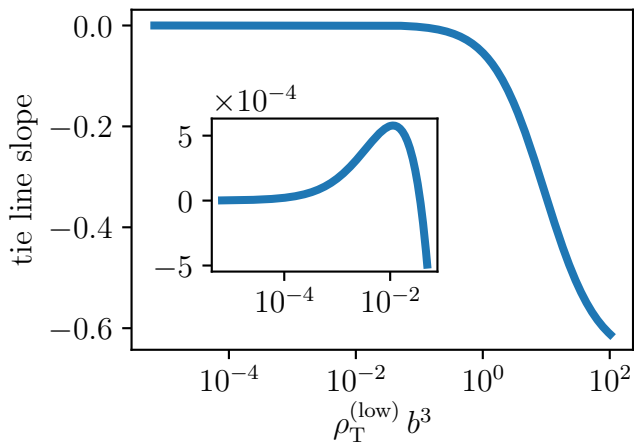


FIG. 4. Slopes of the tielines for the $\gamma = 1.5$ and $l_B = 0.9b$ phase diagram in Fig. 3 (d), as function of the ρ_T value of the polymer-dilute phase. Inset shows the region where tie-line slope changes sign.

of the single unit partition functions stabilized around constant values and the production phase of the simulations were run until a reasonably small standard deviation of the computed observables, K_d and PMFs, were reached. In Fig. 6a, we show representative snapshots of the field picture polymer bead density $\tilde{\rho}_b(\mathbf{r})$, defined in Eq. (28), at different reactant densities for $\gamma = 1.5, 2$

and 2.5 . Consistent with the RPA phase diagrams of Fig. 3, we see polymer droplet formation for all three γ values at relatively low reactant concentrations, but at high reactant concentrations, droplet formation happens only at $\gamma = 1.5$. Different LLPS behavior is also evident from the polymer-polymer PMF plots shown in Figs. 6b–d where at the highest reactant concentrations shown, the PMFs go to zero for $\gamma = 2$ and 2.5 and to a small but non-trivial positive value for $\gamma = 1.5$ at large separations. The short-range effective attraction between polymers and solvated ions or repulsion between polymers and bound AB molecules, respectively, demonstrated by the corresponding PMFs in Fig. 6e–f, are consistent with the tie-line slopes (see Fig. 4) which tend to be positive and negative when ions are in their solvated and bound states, respectively.

VI. CONCLUSIONS

In this work, we have introduced a model for polyampholytes undergoing LLPS in presence of monovalent reactants A^+ and B^- that can form a chemically distinct bound state AB. The dissociated ions have diametrically different effects on the polymer phase separation from their electrically neutral bound counterpart: While the free ions screen the LLPS driving electrostatic interactions between the chains (thus decreasing the phase separation propensity), the bound pairs AB instead func-

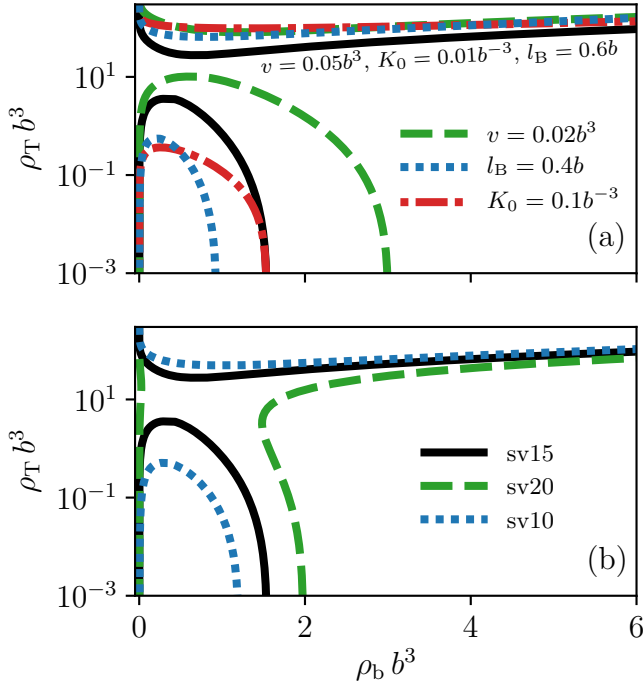


FIG. 5. Re-entrant phase behaviour dependencies on (a) model parameters and (b) polyampholyte charge sequence. The black curve in (a) and (b) correspond to the reference sv15 phase diagram for $\gamma = 1.5$ and $l_B = 0.6b$ in Fig. 3 (top left). Other curves in (a) correspond to varying either v , l_B and K_0 . Other curves in (b) instead show the charge sequence dependence (sequences used are shown in Fig. 1).

tion as a crowding agent that promotes LLPS. Conversely, the crowded and highly charged environment inside the polyampholyte condensates have non-trivial effects on the A – B dissociation constant compared to the co-existing dilute phase. This complex interplay between polymer phase separation and ion dissociation is studied using both analytical and simulation approaches which, in particular, consistently point towards a novel mechanism for re-entrant phase behavior under the circumstances where bound ion pairs yield favorable excluded volume interactions over their dissociated counterpart.

Among the plethora of biological functions of IDP condensates that are currently being uncovered, regulating chemical reactions seem to be one of their major functional roles³⁰. Additionally, chemical reactions in the cellular environment have been shown to be able to both dissolve condensates and trigger their formation^{76–80}. The field theoretic approach presented in this work constitutes a major methodological advancement for modelling of such phenomena, due to our treatment of fluctuations compared to existing MFT theories for polymer phase separation in chemically reactive environments. Accounting for field fluctuations is necessary to capture amino-acid sequence dependence²⁰, and is essential for describing phase separation driven by the electrostatic

interactions³³ characterized by many IDP species.

The proposed mechanism for ion-triggered re-entrant phase separation relies on electrostatic screening from solvated ions A^+/B^- combined with crowding effects from their electrically neutral bound state AB. While Coulombic screening is a long established consequence from free ions, LLPS promoted by molecular crowding is a relatively less so studied phenomenon^{19,38,81,82}. Our model connects these two effects through ion association, quantified by the bare dissociation constant K_0 . Although it remains to be seen if this particular mechanism for re-entrance is realized in nature, we nevertheless believe that our framework for including chemical reactions in RPA and FTS will be applicable to a wide range of systems through minor phenomenological modifications.

ACKNOWLEDGMENTS

The authors thank Yi-Hsuan Lin and Suman Das for insightful discussions. This work was supported by Canadian Institutes of Health Research grant NJT-155930 and Natural Sciences and Engineering Research Council of Canada grant RGPIN-2018-04351 as well as computational resources provided generously by Compute/Calcul Canada. The data that support the findings of this study are available from the corresponding authors upon reasonable request. J.W. and T.P. contributed equally to this work.

Appendix A: Calculation of the sum over n_{AB} in deriving the field Hamiltonian

Here, we show how the sum $S[w, \psi]$ over bound ion pairs n_{AB} in Eq. (12) is computed in the thermodynamic limit. We express $S[w, \psi]$ as

$$S = \sum_{n_{AB}=0}^{n_T} \frac{y^{n_{AB}}}{n_{AB}![(n_T - n_{AB})!]^2}, \quad y \equiv \frac{Q_{AB}}{K_0 V Q_A Q_B}.$$

In the thermodynamic limit, we can replace the sum by an integral which we solve in the saddle-point approximation,

$$S = \int_0^{n_T} dn_{AB} e^{-I(n_{AB})} = e^{-I(n_{AB}^*)},$$

where

$$I(n_{AB}) = \ln n_{AB}! + 2 \ln(n_T - n_{AB})! - n_{AB} \ln y,$$

and n_{AB}^* satisfies the saddle condition $I'(n_{AB}^*) = 0$. Using Stirling's approximation $\ln n! \approx n \ln n - n$ on the logarithm of the factorials gives the saddle condition

$$y = \frac{n_{AB}^*}{(n_T - n_{AB}^*)^2},$$

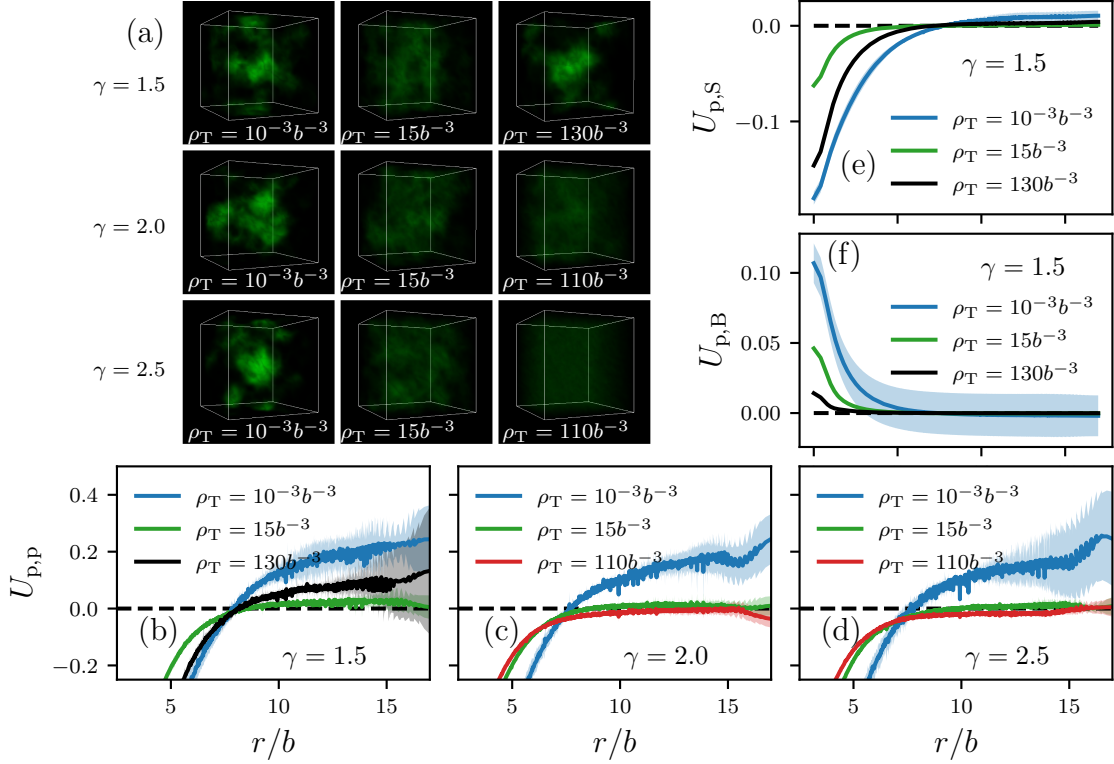


FIG. 6. FTS results for the species sv15 at $l_B = 0.6b$, $\rho_b = 0.1b^{-3}$, $K_0 = 0.01b^{-3}$ and $v = 0.05b^3$. (a) Representative snapshots of real non-negative parts of polymer bead density operator $\tilde{\rho}_b$ at various total bulk ion-densities. (b-d) Polymer-Polymer PMFs at $\gamma = 1.5, 2$ and 2.5 . (e) and (f) Polymer-Solvated-ions PMFs and Polymer-ion-pairs PMFs, respectively, at $\gamma = 1.5$. The solid lines and the shaded regions around the solid lines are mean values and standard deviations of the respective observables computed over five independent simulations, respectively.

which has two solutions,

$$n_{AB}^* = n_T \left[1 + \frac{1 \pm \sqrt{1 + 2x}}{x} \right], \quad x = 2n_T y.$$

However, only the ‘-’ solution is contained in the integration interval $0 \leq n_{AB} \leq n_T$ and contributes to $S[w, \psi]$. Plugging this solution into $I(n_{AB}^*)$ gives

$$I(n_{AB}^*) = \ln n_T! - n_T \ln y + n_T h_0(x),$$

where we again have used Stirling’s approximation in writing $n_T \ln n_T - n_T \approx \ln n_T!$. The function $h_0(x)$ is defined in Eq. (18). The thermodynamic limit of $S[w, \psi]$ then becomes

$$S[w, \psi] = \frac{1}{n_T!} \left[\frac{Q_{AB}}{K_0 V Q_A Q_B} \right]^{n_T} e^{-n_T h_0(x)}.$$

Plugging this expression into Eq. (11) gives the final field representation of the partition function in Eq. (15).

Appendix B: Complete RPA expressions for $\mu_{p,T}$, Π and K_d

This appendix describes the derivation of the RPA expressions for the chemical potentials, osmotic pressure

and dissociation constant. We start by expanding the field Hamiltonian in Eq. (16) around the mean field solution \bar{w} given in Eq. (22). To achieve this, we write

$$w(\mathbf{r}) = \bar{w} + \phi_0 + \phi(\mathbf{r}),$$

with $\int d\mathbf{r} \phi(\mathbf{r}) \equiv 0$ and ϕ_0 is the $\mathbf{k} = \mathbf{0}$ fluctuation mode. In this field basis, the single molecule partition functions defined in Eqs. (13) and (14) become

$$\begin{aligned} Q_p[\check{w}, \check{\psi}] &= e^{-iN(\bar{w} + \phi_0)} Q_p[\check{\phi}, \check{\psi}], \\ Q_{A,B}[\check{w}, \check{\psi}] &= e^{-i(\bar{w} + \phi_0)} Q_{A,B}[\check{\phi}, \check{\psi}], \\ Q_{AB}[\check{w}, \check{\psi}] &= e^{-i\gamma(\bar{w} + \phi_0)} Q_{AB}[\check{\phi}, \check{\psi}]. \end{aligned}$$

Charge neutrality results in a global shift symmetry $\psi(\mathbf{r}) \rightarrow \psi(\mathbf{r}) + (\text{const.})$ that can be used to eliminate the $\mathbf{k} = \mathbf{0}$ mode of $\psi(\mathbf{r})$, such that we can assume $\int d\mathbf{r} \psi(\mathbf{r}) = 0$ in what follows. The single molecule partition functions $Q_i[\check{\phi}, \check{\psi}]$ have the quadratic expansions

$$Q_i[\check{\phi}, \check{\psi}] \approx 1 - \frac{1}{2V} \int \frac{d\mathbf{k}}{(2\pi)^3} \Psi^T(-\mathbf{k}) G_i \Psi(\mathbf{k}),$$

for $i = p, A, B, AB$, with $\Psi(\mathbf{k}) = (\check{\phi}(\mathbf{k}), \check{\psi}(\mathbf{k}))^T$ containing the Fourier transformed field fluctuations. Here, G_p

is defined as in the main text and

$$\mathbf{G}_{A,B} = \hat{\Gamma}^2 \begin{pmatrix} 1 & \pm 1 \\ \pm 1 & 1 \end{pmatrix}, \quad \mathbf{G}_{AB} = \hat{\Gamma}^2 \begin{pmatrix} \gamma^2 & 0 \\ 0 & 0 \end{pmatrix}.$$

To find the RPA expansion of the term $n_{\text{T}}h_0(x[w, \psi])$ in the field Hamiltonian, we first express the expansion of the field operator $x[w, \psi]$, defined in Eq. (17), as

$$x[w, \psi] \approx \bar{x}e^{(2-\gamma)i\phi_0}(1 + \epsilon) \equiv x_0(1 + \epsilon),$$

with $\bar{x} = 2\rho_{\text{T}}e^{(2-\gamma)i\bar{w}}/K_0$ and $\epsilon \equiv \int d\mathbf{k}\Psi(-\mathbf{k})^{\text{T}}(\mathbf{G}_A + \mathbf{G}_B - \mathbf{G}_{AB})\Psi(\mathbf{k})/2V(2\pi)^3$. The RPA expansion of $h_0(x)$ simplifies to $h_0(x) \approx h_0(x_0) + h_1(x_0)\epsilon \approx h_0(x_0) + \bar{h}_1\epsilon$ with $\bar{h}_i \equiv h_i(\bar{x})$. The expansion of $h_0(x_0)$ to quadratic order in ϕ_0 becomes $h_0(x_0) \approx \bar{h}_0 + (2-\gamma)\bar{h}_1i\phi_0 - (2-\gamma)^2\bar{h}_2\phi_0^2$. This last step can be obtained using the relation $h_0''(x)x^2 = h_2(x) - h_1(x)$ which can be proven by considering $(h_1(x)x)'$ and $h_{i+1}(x) \equiv h_i'(x)x$.

Combining the above expansion of $h_0(x)$ with the expansion of the other terms in Eq. (16) leads to the RPA expansion of the field Hamiltonian $H[w, \psi] \approx H[\bar{w}, 0] + H^{(\text{RPA})}$ with

$$H^{(\text{RPA})} = -\frac{n_{\text{T}}}{2}(2-\gamma)^2\bar{h}_2\phi_0^2 + \frac{1}{2} \int \frac{d\mathbf{k}}{(2\pi)^3} \Psi(-\mathbf{k})^{\text{T}} \mathbf{G} \Psi(\mathbf{k})$$

where \mathbf{G} is defined as in the main text. One can show that the contribution from ϕ_0 vanishes in the infinite volume limit ($V \rightarrow \infty$), and will therefore be omitted in the following RPA calculations. Note, however, that the

quadratic expansion of $H[w, \psi]$ is also used for the semi-implicit CL time integration used in FTS, which accounts for the $\mathbf{k} = \mathbf{0}$ modes explicitly.

Performing the Gaussian field integrals over $\phi(\mathbf{r})$ and $\psi(\mathbf{r})$ leads to the RPA free energy density in Eq. (25), $f \approx \bar{f} + f^{(\text{fl})}$ with

$$f^{(\text{fl})} = \frac{1}{4\pi^2} \int_0^\infty dk k^2 \ln \left(\frac{4\pi l_{\text{B}} v}{k^2} \det \mathbf{G} \right).$$

The derivatives required for the RPA chemical potentials are

$$\frac{\partial f^{(\text{fl})}}{\partial \rho_i} = \frac{1}{4\pi^2} \int_0^\infty dk k^2 \text{Tr} \left[\mathbf{G}^{-1} \frac{\partial \mathbf{G}}{\partial \rho_i} \right], \quad i = \text{b, T}.$$

The density derivatives of the matrix \mathbf{G} includes contributions from the derivatives of the MFT bound fraction \bar{h}_1 ,

$$\begin{aligned} \rho_{\text{T}} \frac{\partial \bar{h}_1}{\partial \rho_{\text{b}}} &= \frac{(2-\gamma)\bar{h}_2\rho_{\text{T}}v}{1 - (2-\gamma)^2\bar{h}_2\rho_{\text{T}}v}, \\ \rho_{\text{T}} \frac{\partial \bar{h}_1}{\partial \rho_{\text{T}}} &= \bar{h}_2 \left[1 + (2-\gamma)\rho_{\text{T}}v \frac{\gamma + (2-\gamma)(\bar{h}_1 + \bar{h}_2)}{1 - (2-\gamma)^2\bar{h}_2\rho_{\text{T}}v} \right], \end{aligned}$$

which can be derived by taking the corresponding derivatives of Eq. (22). The resulting RPA contributions for the chemical potentials, $\mu_{\text{p}}^{(\text{fl})} = N\partial f^{(\text{fl})}/\partial \rho_{\text{b}}$ and $\mu_{\text{T}}^{(\text{fl})} = \partial f^{(\text{fl})}/\partial \rho_{\text{T}}$, become

$$\begin{aligned} \mu_{\text{p}}^{(\text{fl})} &= \frac{N}{4\pi^2} \int_0^\infty dk k^2 \text{Tr} \left\{ \mathbf{G}^{-1} \left[\mathbf{G}_{\text{p}} + \frac{(2-\gamma)\bar{h}_2\rho_{\text{T}}v}{1 - (2-\gamma)^2\bar{h}_2\rho_{\text{T}}v} (\mathbf{G}_A + \mathbf{G}_B - \mathbf{G}_{AB}) \right] \right\}, \\ \mu_{\text{T}}^{(\text{fl})} &= \frac{1}{4\pi^2} \int_0^\infty dk k^2 \text{Tr} \left\{ \mathbf{G}^{-1} \left[\mathbf{G}_{\text{T}} + \bar{h}_2 \left(1 + (2-\gamma)\rho_{\text{T}}v \frac{\gamma + (2-\gamma)(\bar{h}_1 + \bar{h}_2)}{1 - (2-\gamma)^2\bar{h}_2\rho_{\text{T}}v} \right) (\mathbf{G}_A + \mathbf{G}_B - \mathbf{G}_{AB}) \right] \right\}. \end{aligned}$$

The fluctuation contribution to the osmotic pressure can then be obtained as $\Pi^{(\text{fl})} = \rho_{\text{b}}\mu_{\text{p}}^{(\text{fl})}/N + \rho_{\text{T}}\mu_{\text{T}}^{(\text{fl})} - f^{(\text{fl})}$.

The RPA expression for the density of dissociated ions $[A^+]$ follows from Eq. (10),

$$[A^+] = \bar{h}_1\rho_{\text{T}} - \frac{1}{4\pi^2} \int_0^\infty dk k^2 \text{Tr} \left[\mathbf{G}^{-1} K_0 \frac{\partial \mathbf{G}}{\partial K_0} \right],$$

with

$$K_0 \frac{\partial \mathbf{G}}{\partial K_0} = -\frac{\rho_{\text{T}}\bar{h}_2(\mathbf{G}_A + \mathbf{G}_B - \mathbf{G}_{AB})}{1 - (2-\gamma)^2\rho_{\text{T}}v\bar{h}_2}.$$

The resulting RPA formula for the fraction of dissociated ions becomes $\langle h_1(x) \rangle = \bar{h}_1 + h_1^{(\text{fl})}$ with

$$h_1^{(\text{fl})} = \frac{\bar{h}_2 \int_0^\infty dk k^2 \text{Tr} \left[\mathbf{G}^{-1} (\mathbf{G}_A + \mathbf{G}_B - \mathbf{G}_{AB}) \right]}{4\pi^2 (1 - (2-\gamma)^2\rho_{\text{T}}v\bar{h}_2)},$$

which can be plugged into Eq. (21) to obtain the RPA dissociation constant.

Appendix C: Detailed expressions of the density operators used FTS

For a given field configuration $\{w(\mathbf{r}), \psi(\mathbf{r})\}$, the forward and backward propagators $q_{\text{F}}(\mathbf{r}, \alpha)$ and $q_{\text{B}}(\mathbf{r}, \alpha)$, respectively, associated with the discrete bead-spring polymer chain model used in this work can be used to calculate the field operators $\tilde{\rho}_{\text{p}}(\mathbf{r})$, $\tilde{c}_{\text{p}}(\mathbf{r})$ and $Q_{\text{p}}[\tilde{w}, \tilde{\psi}]$. The chain propagators are constructed iteratively through Kolmogorov–Chapman equations as

$$\begin{aligned} q_{\text{F}}(\mathbf{r}, \alpha + 1) &= e^{-iW(\mathbf{r}, \alpha + 1)} \Phi \star q_{\text{F}}(\mathbf{r}, \alpha), \\ q_{\text{B}}(\mathbf{r}, \alpha - 1) &= e^{-iW(\mathbf{r}, \alpha - 1)} \Phi \star q_{\text{B}}(\mathbf{r}, \alpha), \end{aligned}$$

where $W(\mathbf{r}, \alpha) \equiv \check{w}(\mathbf{r}) + \sigma_\alpha \check{\psi}(\mathbf{r})$, $\Phi(\mathbf{r}) \equiv (3/2\pi b^2)^{3/2} \exp(-3\mathbf{r}^2/2b^2)$, and starting from $q_F(\mathbf{r}, 1) = \exp[-iW(\mathbf{r}, 1)]$ and $q_B(\mathbf{r}, N) = \exp[-iW(\mathbf{r}, N)]$. Here ‘ \star ’ denotes a spatial convolution. One can then show that

$$Q_p[\check{w}, \check{\psi}] = \frac{1}{V} \int d\mathbf{r} q_F(\mathbf{r}, N),$$

$$\tilde{\rho}_b(\mathbf{r}) = \Gamma \star \frac{\rho_b}{N Q_p[\check{w}, \check{\psi}]} \sum_{\alpha=1}^N e^{iW(\mathbf{r}, \alpha)} q_F(\mathbf{r}, \alpha) q_B(\mathbf{r}, \alpha),$$

$$\tilde{c}_b(\mathbf{r}) = \Gamma \star \frac{\rho_b}{N Q_p[\check{w}, \check{\psi}]} \sum_{\alpha=1}^N e^{iW(\mathbf{r}, \alpha)} q_F(\mathbf{r}, \alpha) q_B(\mathbf{r}, \alpha) \sigma_\alpha.$$

Bead density operators for A^+ , B^- and AB are given by

$$\tilde{\rho}_A = h_1(x) \frac{\rho_T}{Q_A[\check{w}, \check{\psi}]} e^{-i\check{w} - i\check{\psi}},$$

$$\tilde{\rho}_B = h_1(x) \frac{\rho_T}{Q_B[\check{w}, \check{\psi}]} e^{-i\check{w} + i\check{\psi}},$$

$$\tilde{\rho}_{AB} = [1 - h_1(x)] \frac{\gamma \rho_T}{Q_{AB}[\check{w}, \check{\psi}]} e^{-i\gamma \check{w}}.$$

¹Clifford P. Brangwynne, Christian R. Eckmann, David S. Courson, Agata Rybarska, Carsten Hoege, Jöbin Gharakhani, Frank Jülicher, and Anthony A. Hyman. Germline p granules are liquid droplets that localize by controlled dissolution/condensation. *Science*, 324(5935):1729–1732, 2009.

²P Li, S Banjade, H C Cheng, S Kim, B Chen, L Guo, M Llaguno, J V Hollingsworth, D S King, S F Banani, P S Russ, Q-X Jiang, B T Nixon, and M K Rosen. Phase transitions in the assembly of multivalent signalling proteins. *Nature*, 483:336–340, 2012.

³M Kato, T W Han, S Xie, K Shi, X Du, L C Wu, H Mirzaei, E J Goldsmith, J Longgood, J Pei, N V Grishin, D E Frantz, J W Schneider, S Chen, L Li, M R Sawaya, D Eisenberg, R Tycko, and S L McKnight. Cell-free formation of rna granules: low complexity sequence domains form dynamic fibers within hydrogels. *Cell*, 149:753–767, 2012.

⁴A A Hyman, C A Weber, and F Jülicher. Liquid-liquid phase separation in biology. *Annu. Rev. Cell Dev. Biol.*, 30:39–58, 2014.

⁵Timothy J Nott, Evangelia Petsalaki, Patrick Farber, Dylan Jarvis, Eden Fussner, Anne Plochowitz, Timothy D Craggs, David P Bazett-Jones, Tony Pawson, Julie D Forman-Kay, and Andrew J Baldwin. Phase transition of a disordered nuage protein generates environmentally responsive membraneless organelles. *Mol. Cell*, 57(5):936–947, Mar 2015.

⁶Salman F Banani, Hyun O Lee, Anthony A Hyman, and Michael K Rosen. Biomolecular condensates: organizers of cellular biochemistry. *Nat. Rev. Mol. Cell. Biol.*, 18:285–298, Oct 2017.

⁷Simon Alberti. Phase separation in biology. *Curr. Biol.*, 27(20):R1097 – R1102, 2017.

⁸Xiao-Han Li, Pavithra L. Chavali, Rita Panca, Sreenivas Chavali, and M. Madan Babu. Function and regulation of phase-separated biological condensates. *Biochemistry*, 57(17):2452–2461, 2018.

⁹Amandine Molliex, Jamshid Temirov, Jihun Lee, Maura Coughlin, Anderson P. Kanagaraj, Hong Joo Kim, Tanja Mittag, and J. Paul Taylor. Phase separation by low complexity domains promotes stress granule assembly and drives pathological fibrillization. *Cell*, 163(1):123 – 133, 2015.

¹⁰C P Brangwynne, P Tompa, and R V Pappu. Polymer physics of intracellular phase transitions. *Nat. Phys.*, 11:899–904, 2015.

¹¹P Andrew Chong and Julie D Forman-Kay. Liquid-liquid phase separation in cellular signaling systems. *Curr. Opin. Struct. Biol.*, 41:180–186, 2016.

¹²Salman F Banani, Hyun O Lee, Anthony A Hyman, and Michael K Rosen. Biomolecular condensates: Organizers of cellular biochemistry. *Nat. Rev. Mol. Cell Biol.*, 18(5):285–298, May 2017.

¹³X Chen, X Wu, H Wu, and M Zhang. Phase transition at the synapse. *Nat. Neurosci.*, 23:301–310, 2020.

¹⁴V N Uversky. Natively unfolded proteins: A point where biology waits for physics. *Protein Sci.*, 11(4):739–756, 2002.

¹⁵T Chen, J Song, and H S Chan. Theoretical perspectives on nonnative interactions and intrinsic disorder in protein folding and binding. *Curr. Opin. Struct. Biol.*, 30:32–42, 2015.

¹⁶Robert McCoy Vernon, Paul Andrew Chong, Brian Tsang, Tae Hun Kim, Alaji Bah, Patrick Farber, Hong Lin, and Julie Deborah Forman-Kay. Pi-pi contacts are an overlooked protein feature relevant to phase separation. *eLife*, 7:e31486, feb 2018.

¹⁷Suman Das, Yi-Hsuan Lin, Robert M. Vernon, Julie D. Forman-Kay, and Hue Sun Chan. Comparative roles of charge, π , and hydrophobic interactions in sequence-dependent phase separation of intrinsically disordered proteins. *Proceedings of the National Academy of Sciences*, 2020.

¹⁸Suman Das, Adam Eisen, Yi-Hsuan Lin, and Hue Sun Chan. A lattice model of charge-pattern-dependent polyampholyte phase separation. *The Journal of Physical Chemistry B*, 122(21):5418–5431, 2018. PMID: 29397728.

¹⁹Jonas Wessén, Tanmoy Pal, Suman Das, Yi-Hsuan Lin, and Hue Sun Chan. A simple explicit-solvent model of polyampholyte phase behaviors and its ramifications for dielectric effects in biomolecular condensates. *The Journal of Physical Chemistry B*, 125(17):4337–4358, 2021. PMID: 33890467.

²⁰Yi-Hsuan Lin, Julie D. Forman-Kay, and Hue Sun Chan. Sequence-specific polyampholyte phase separation in membraneless organelles. *Phys. Rev. Lett.*, 117:178101, Oct 2016.

²¹James McCarty, Kris T. Delaney, Scott P. O. Danielsen, Glenn H. Fredrickson, and Joan-Emma Shea. Complete phase diagram for liquid-liquid phase separation of intrinsically disordered proteins. Mar 2019.

²²S Cinar, H Cinar, H S Chan, and R Winter. Pressure-sensitive and osmolyte-modulated liquid-liquid phase separation of eye-lens γ -crystallins. *J. Am. Chem. Soc.*, 141:7347–7354, 2019.

²³G L Dignon, W Zheng, Y C Kim, and J Mittal. Temperature-controlled liquid-liquid phase separation of disordered proteins. *ACS Cent. Sci.*, 5:821–830, 2019.

²⁴H Cinar, R Oliva, Y-H Lin, X Chen, M Zhang, H S Chan, and R Winter. Pressure sensitivity of syngap/psd-95 condensates as a model for postsynaptic densities and its biophysical and neurological ramifications. *Chem Eur. J.*, 26:11024–11031, 2020.

²⁵Zamira Fetahaj, Lena Ostermeier, Hasan Cinar, Rosario Oliva, and Roland Winter. Biomolecular condensates under extreme martian salt conditions. *Journal of the American Chemical Society*, 143(13):5247–5259, 2021. PMID: 33755443.

²⁶Omar Adame-Arana, Christoph A. Weber, Vasily Ziburdaev, Jacques Prost, and Frank Jülicher. Liquid phase separation controlled by ph. *Biophysical Journal*, 119(8):1590–1605, Oct 2020.

²⁷Adiran Garaizar and Jorge R. Espinosa. Salt dependent phase behavior of intrinsically disordered proteins from a coarse-grained model with explicit water and ions. *The Journal of Chemical Physics*, 155(12):125103, 2021.

²⁸Georg Krainer, Timothy Welsh, Jerelle Joseph, Jorge Espinosa, Ella Csillery, Akshay Sridhar, Zenon Toprakcioglu, Giedre Gudiskyte, Magdalena Czekalska, William Arter, Peter George-Hyslop, Rosana Collepardo-Guevara, Simon Alberti, and Thomas Knowles. Reentrant liquid condensate phase of proteins is stabilized by hydrophobic and non-ionic interactions. 05 2020.

²⁹Kibeom Hong, Daesun Song, and Yongwon Jung. Behavior control of membrane-less protein liquid condensates with metal ion-induced phase separation. *Nature Communications*, 11(1), nov

- 2020.
- ³⁰Simon Alberti, Amy Gladfelter, and Tanja Mittag. Considerations and challenges in studying liquid-liquid phase separation and biomolecular condensates. *Cell*, 176(3):419–434, 2019.
- ³¹Yi-Hsuan Lin, Haowei Wu, Bowen Jia, Mingjie Zhang, and Hue Sun Chan. Assembly of model postsynaptic densities involves interactions auxiliary to stoichiometric binding. *Biophysical Journal*, 2021.
- ³²Giacomo Bartolucci, Omar Adame-Arana, Xueping Zhao, and Christoph A. Weber. Controlling composition of coexisting phases via molecular transitions. *Biophysical Journal*, 120(21):4682–4697, 2021.
- ³³Yuri O. Popov, Jonghoon Lee, and Glenn H. Fredrickson. Field-theoretic simulations of polyelectrolyte complexation. *Journal of Polymer Science Part B: Polymer Physics*, 45(24):3223–3230, 2007.
- ³⁴Chantal Valeriani, Philip J. Camp, Jos W. Zwanikken, René van Roij, and Marjolein Dijkstra. Ion association in low-polarity solvents: comparisons between theory, simulation, and experiment. *Soft Matter*, 6:2793–2800, 2010.
- ³⁵Thomas G. Spiro, Agnes Revesz, and Judith Lee. Volume changes in ion association reactions. inner- and outer-sphere complexes. *Journal of the American Chemical Society*, 90(15):4000–4006, 1968.
- ³⁶Stacey E. Wark, Chih-Hao Hsia, and Dong Hee Son. Effects of ion solvation and volume change of reaction on the equilibrium and morphology in cation-exchange reaction of nanocrystals. *Journal of the American Chemical Society*, 130(29):9550–9555, 2008. PMID: 18588299.
- ³⁷Y. Marcus. The volume change on ion-pairing of symmetrical electrolytes. *Zeitschrift für Naturforschung A*, 38(2):247–251, 1983.
- ³⁸Sohee Park, Ryan Barnes, Yanxian Lin, Byoung-jin Jeon, Saeed Najafi, Kris Delaney, Glenn Fredrickson, Joan Shea, Dong Hwang, and Songi Han. Dehydration entropy drives liquid-liquid phase separation by molecular crowding. *Communications Chemistry*, 3:83, 06 2020.
- ³⁹P. González-Mozuelos and M. Olvera de la Cruz. Random phase approximation for complex charged systems: Application to copolyelectrolytes (polyampholytes). *The Journal of Chemical Physics*, 100(1):507–517, 1994.
- ⁴⁰Rahul K. Das and Rohit V. Pappu. Conformations of intrinsically disordered proteins are influenced by linear sequence distributions of oppositely charged residues. *Proceedings of the National Academy of Sciences*, 110(33):13392–13397, 2013.
- ⁴¹Suman Das, Alan N. Amin, Yi-Hsuan Lin, and Hue Sun Chan. Coarse-grained residue-based models of disordered protein condensates: utility and limitations of simple charge pattern parameters. *Phys. Chem. Chem. Phys.*, 20:28558–28574, 2018.
- ⁴²Tanmoy Pal, Jonas Wessén, Suman Das, and Hue Sun Chan. Subcompartmentalization of polyampholyte species in organelle-like condensates is promoted by charge-pattern mismatch and strong excluded-volume interaction. *Phys. Rev. E*, 103:042406, Apr 2021.
- ⁴³Yi-Hsuan Lin, Jonas Wessén, Tanmoy Pal, Suman Das, and Hue Sun Chan. Numerical techniques for applications of analytical theories to sequence-dependent phase separations of intrinsically disordered proteins. *Methods in Molecular Biology (Springer-Nature)*, accepted for publication, arXiv:2201.01920, 2022.
- ⁴⁴Lucas Sawle and Kingshuk Ghosh. A theoretical method to compute sequence dependent configurational properties in charged polymers and proteins. *The Journal of Chemical Physics*, 143(8):085101, 2015.
- ⁴⁵Jason J. Madinya, Li-Wei Chang, Sarah L. Perry, and Charles E. Sing. Sequence-dependent self-coacervation in high charge-density polyampholytes. *Mol. Syst. Des. Eng.*, 5:632–644, 2020.
- ⁴⁶Ali Salehi and Ronald G. Larson. A molecular thermodynamic model of complexation in mixtures of oppositely charged polyelectrolytes with explicit account of charge association/dissociation. *Macromolecules*, 49(24):9706–9719, 2016.
- ⁴⁷Sean Friedowitz, Ali Salehi, Ronald G. Larson, and Jian Qin. Role of electrostatic correlations in polyelectrolyte charge association. *The Journal of Chemical Physics*, 149(16):163335, 2018.
- ⁴⁸Mohsen Ghasemi, Sean Friedowitz, and Ronald G. Larson. Analysis of partitioning of salt through doping of polyelectrolyte complex coacervates. *Macromolecules*, 53(16):6928–6945, 2020.
- ⁴⁹Charles E. Sing. Micro- to macro-phase separation transition in sequence-defined coacervates. *The Journal of Chemical Physics*, 152(2):024902, 2020.
- ⁵⁰Ashley R. Knoerdel, Whitney C. Blocher McTigue, and Charles E. Sing. Transfer matrix model of ph effects in polymeric complex coacervation. *The Journal of Physical Chemistry B*, 125(31):8965–8980, 2021. PMID: 34328340.
- ⁵¹W. G. Noid. Perspective: Coarse-grained models for biomolecular systems. *The Journal of Chemical Physics*, 139(9):090901, 2013.
- ⁵²Zhen-Gang Wang. Fluctuation in electrolyte solutions: The self energy. *Phys. Rev. E*, 81:021501, Feb 2010.
- ⁵³Robert A. Riggelman, Rajeev Kumar, and Glenn H. Fredrickson. Investigation of the interfacial tension of complex coacervates using field-theoretic simulations. *The Journal of Chemical Physics*, 136(2):024903, 2012.
- ⁵⁴Scott P. O. Danielsen, James McCarty, Joan-Emma Shea, Kris T. Delaney, and Glenn H. Fredrickson. Molecular design of self-coacervation phenomena in block polyampholytes. *Proceedings of the National Academy of Sciences*, 116(17):8224–8232, 2019.
- ⁵⁵M. Olvera de la Cruz, L. Belloni, M. Delsanti, J. P. Dalbiez, O. Spalla, and M. Drifford. Precipitation of highly charged polyelectrolyte solutions in the presence of multivalent salts. *The Journal of Chemical Physics*, 103(13):5781–5791, 1995.
- ⁵⁶Alexander Kudlay, Alexander V. Ermoshkin, and Monica Olvera de la Cruz. Complexation of oppositely charged polyelectrolytes: Effect of ion pair formation. *Macromolecules*, 37(24):9231–9241, 2004.
- ⁵⁷Alexander Kudlay and Monica Olvera de la Cruz. Precipitation of oppositely charged polyelectrolytes in salt solutions. *The Journal of Chemical Physics*, 120(1):404–412, 2004.
- ⁵⁸Keith J Laidler. *Chemical kinetics*. Number 544.4 LAI. 1987.
- ⁵⁹R. P. Buck, S. Rondinini, A. K. Covington, F. G. K. Baucke, Christopher M. A. Brett, M. F. Camoes, M. J. T. Milton, T. Mussini, R. Naumann, K. W. Pratt, P. Spitzer, and G. S. Wilson. Measurement of ph. definition, standards, and procedures (iupac recommendations 2002). *Pure and Applied Chemistry*, 74(11):2169–2200, 2002.
- ⁶⁰S F Edwards. The statistical mechanics of polymers with excluded volume. *Proceedings of the Physical Society*, 85(4):613–624, apr 1965.
- ⁶¹Glenn Fredrickson. *The equilibrium theory of inhomogeneous polymers*, volume 134. Oxford University Press on Demand, 2006.
- ⁶²Michael C Villet and Glenn H Fredrickson. Efficient field-theoretic simulation of polymer solutions. *J. Chem. Phys.*, 141(22):224115, Dec 2014.
- ⁶³Kevin S. Silmore, Michael P. Howard, and Athanassios Z. Panagiotopoulos. Vapour–liquid phase equilibrium and surface tension of fully flexible lennard–jones chains. *Molecular Physics*, 115(3):320–327, 2017.
- ⁶⁴Gregory L. Dignon, Wenwei Zheng, Young C. Kim, Robert B. Best, and Jeetain Mittal. Sequence determinants of protein phase behavior from a coarse-grained model. *PLOS Computational Biology*, 14(1):1–23, 01 2018.
- ⁶⁵Daniel Nilsson and Anders Irback. Finite-size scaling analysis of protein droplet formation. *Phys. Rev. E*, 101:022413, Feb 2020.
- ⁶⁶Daniel Nilsson and Anders Irback. Finite-size shifts in simulated protein droplet phase diagrams. *The Journal of Chemical Physics*, 154(23):235101, 2021.
- ⁶⁷G H Fredrickson, V Ganesan, and F Drolet. Field-theoretic computer simulation methods for polymers and complex fluids. *Macromolecules*, 35:16–39, 2002.
- ⁶⁸G Parisi and Y-S Wu. Perturbation theory without gauge fixing.

- Sci. Sinica*, 24:483–496, 1981.
- ⁶⁹G Parisi. On complex probabilities. *Phys. Lett. B*, 131(4):393 – 395, 1983.
- ⁷⁰J R Klauder. A langevin approach to fermion and quantum spin correlation functions. *J. Phys. A: Math. Gen.*, 16(10):L317–L319, jul 1983.
- ⁷¹H S Chan and M B Halpern. New ghost-free infrared-soft gauges. *Phys. Rev. D*, 33:540–547, 1986.
- ⁷²Erin M. Lennon, George O. Mohler, Hector D. Ceniceros, Carlos J. García-Cervera, and Glenn H. Fredrickson. Numerical solutions of the complex langevin equations in polymer field theory. *Multiscale Modeling & Simulation*, 6(4):1347–1370, 2008.
- ⁷³Daniel Nilsson, Behruz Bozorg, Sandipan Mohanty, Bo Söderberg, and Anders Irbäck. Limitations of field-theory simulation for exploring phase separation: The role of repulsion in a lattice protein model. *The Journal of Chemical Physics*, 156(1):015101, 2022.
- ⁷⁴Mehran Kardar. *Statistical Physics of Particles*. Cambridge University Press, 2007.
- ⁷⁵Rahul K. Das and Rohit V. Pappu. Conformations of intrinsically disordered proteins are influenced by linear sequence distributions of oppositely charged residues. *Proceedings of the National Academy of Sciences*, 110(33):13392–13397, 2013.
- ⁷⁶Frank Wippich, Bernd Bodenmiller, Maria Gustafsson Trajkovska, Stefanie Wanka, Ruedi Aebersold, and Lucas Pelkmans. Dual specificity kinase dyrk3 couples stress granule condensation/dissolution to mtorc1 signaling. *Cell*, 152(4):791–805, 2013.
- ⁷⁷David Zwicker, Anthony A. Hyman, and Frank Jülicher. Suppression of ostwald ripening in active emulsions. *Phys. Rev. E*, 92:012317, Jul 2015.
- ⁷⁸David Zwicker, Rabea Seyboldt, Christoph A Weber, Anthony A Hyman, and Frank Jülicher. Growth and division of active droplets provides a model for protocells. *Nature Physics*, 13(4):408–413, 2017.
- ⁷⁹Jean David Wurtz and Chiu Fan Lee. Chemical-reaction-controlled phase separated drops: Formation, size selection, and coarsening. *Phys. Rev. Lett.*, 120:078102, Feb 2018.
- ⁸⁰Jan Kirschbaum and David Zwicker. Controlling biomolecular condensates via chemical reactions. *Journal of The Royal Society Interface*, 18(179):20210255, 2021.
- ⁸¹Hue Sun Chan and Ken A Dill. Solvation: how to obtain microscopic energies from partitioning and solvation experiments. *Annual review of biophysics and biomolecular structure*, 26(1):425–459, 1997.
- ⁸²Ashoka Ray. Solvophobic interactions and micelle formation in structure forming nonaqueous solvents. *Nature*, 231(5301):313–315, 1971.